ADVANCED ENERGY & SUSTAINABILITY RESEARCH
www.advenergysustres.com

# Perfluoroarene-Based Tin Halide Perovskite Photovoltaics

*Mengqiong Zhu, Shivam Singh, Alejandra Maria Castro Chong, Jong-Min Kim, Fulya Koc, Debendra Prasad Panda, Paul Zimmermann, Alexander Hinderhofer, Weifan Luo, Ghewa Alsabeh, Muhammad Okash Ur Rehman, Gyeongcheon Choi, Dmitry Chernyshov, Frank Schreiber, Ji-Youn Seo, Yana Vaynzof, Antonio Abate,* and Jovana V. Milić**

**Hybrid halide perovskites are among the most promising candidates for next-generation photovoltaics. The most investigated perovskite solar cells are lead based, which poses environmental concerns, making finding sustainable alternatives a pressing issue. Tin-based halide perovskites are attracting interest as an alternative. However, their application in photovoltaics is hindered by the high concentration of defects and sensitivity to oxidation, compromising their performance and stability. Herein, perfluoroarene organic cations, namely 2-(perfluorophenyl)methylammonium (F-BNA) and 1,4-(perfluorophenyl)dimethylammonium (F-PDMA), are applied to form layered (2D) Ruddlesden–Popper and Dion–Jacobson tin-based perovskites, respectively. Following a detailed structural and optoelectronic characterization, the perfluoroarenes are applied to formamidinium (FA)-based $FASnI_3$ perovskite solar cells and an effective solvent is identified for their processing, 2-pentanol. While F-PDMA forms a 2D/3D heterostructure, F-BNA remains assembled as a molecular interlayer, demonstrating higher photovoltaic performance with limited operational stability. This challenges the conventional role of mixed-dimensional heterostructures in tin perovskite photovoltaics and opens new perspectives for advanced material design and device engineering.**

## 1. Introduction

Hybrid halide perovskites have emerged as leading semiconductors for next-generation photovoltaics. However, conventional lead-based perovskite solar cells are environmentally harmful, motivating the search for sustainable alternatives.[1,2] Tin-based (Sn) hybrid perovskites present a suitable alternative due to their lower toxicity and comparable characteristics.[3,4] However, the application of tin-based perovskites in photovoltaics is hindered by their high concentration of defects and sensitivity to oxidation, which compromises solar cell performance and stability.[5–7] While tin-based perovskite solar cells have surpassed 15% in certificated efficiency,[8] their development lags behind their lead analogues due to the fast crystallization and oxidation of Sn(II) to Sn(IV) that affect the perovskite structure, leading to a high concentration of defects and reducing the photovoltaic performances and stability.[9] Efforts to overcome these challenges include compositional, solvent, and interfacial engineering approaches.[5–7] One of the most effective strategies relies on interfacial molecular assemblies and low-dimensional hybrid perovskites based on hydrophobic organic moieties,[5–7] which can be incorporated within the perovskite framework. Layered (2D) tin halide perovskites can be described by $S_2A_{n-1}Sn_nX_{3n+1}$ or $S'A_{n-1}Sn_nX_{3n+1}$ formulae, where A are central cations, X halide anions, and S or S' (typically mono- or bifunctional ammonium cations, respectively) organic spacers, which often form Ruddlesden–Popper (RP) and Dion–Jacobson (DJ) phases.[10] Organic spacer cations template the perovskite slabs with either a displacement by half a unit cell along between adjacent slabs for the RP phase or the absence of displacement in DJ phases.[11] Mixed-dimensional (e.g., 2D/3D)

M. Zhu, W. Luo, G. Alsabeh, J. V. Milić
Adolphe Merkle Institute
University of Fribourg
1700 Fribourg, Switzerland
E-mail: jovana.milic@unifr.ch

The ORCID identification number(s) for the author(s) of this article can be found under https://doi.org/10.1002/aesr.202500028.



DOI: 10.1002/aesr.202500028

S. Singh, A. M. C. Chong, F. Koc, Y. Vaynzof
Chair for Emerging Electronic Technologies
Technische Universität Dresden
Nöthnitzer Straße 61, 01187 Dresden, Germany

S. Singh, A. M. C. Chong, F. Koc, Y. Vaynzof
Leibniz-Institute for Solid State and Materials Research Dresden
Helmholtzstraße 20, 01069 Dresden, Germany

J.-M. Kim, G. Choi, J.-Y. Seo
Department of Nanoenergy Engineering
Pusan National University
Busan 46241, South Korea

structures were shown to achieve superior power conversion efficiencies, facilitate charge transport, and enhance the performance of solar cells.[12–19] Moreover, fluorinated organic moieties have shown potential due to their hydrophobicity and higher electronegativity of fluorine substituents compared to their nonfluorinated analogues, which can affect redox properties and energetics in perovskite photovoltaics.[20,21] However, the material scope remains limited, and there is an interest in establishing design strategies for mixed-dimensional tin perovskite materials in photovoltaics.

In this work, we apply tailored perfluoroarene organic cations, namely 2-(perfluorophenyl)methylammonium (F-BNA) and 1,4-(perfluorophenyl)dimethylammonium (F-PDMA), to form representative RP and DJ 2D Sn perovskite phases, respectively (**Figure 1**). They are investigated by structural and optoelectronic characterization techniques, including X-ray diffraction (XRD), UV–vis absorption, and photoluminescence (PL) spectroscopy, to evidence the formation of 2D Sn perovskite phases. The resulting materials were used for the first time in Sn-based perovskite architectures to form mixed-dimensional perovskite heterostructures by applying F-BNA and F-PDMA as overlayers onto 3D perovskite absorber layers and identifying the optimal solvent for processing (2-pentanol), further optimizing the optoelectronic characteristics and stability. While 2-PDMA was found to form a 2D/3D heterostructure, F-BNA formed a molecular overlayer on the 3D perovskite phase. Finally, the incorporation into p–i–n perovskite solar cells[22] based on indium tin oxide (ITO)/poly(3,4-ethylenedioxythisphene) (PEDOT)/$FASnI_3$/perfluoroarene/$C_{60}$/bathocuproine (BCP)/Ag (Figure 1a) architecture demonstrated improvements in photovoltaic performances with power conversion efficiencies up to 9.1% and enhanced operational stability, offering a new strategy for advancing perovskite photovoltaics.

D. P. Panda, M. O. Ur Rehman, A. Abate
Department of Chemical
Materials and Production Engineering
University of Naples Federico II
Fuorigrotta, Piazzale Via Tecchio 80, 80125 Naples, Italy
E-mail: antonio.abate@unina.it

P. Zimmermann, A. Hinderhofer, F. Schreiber
Institut für Angewandte Physik
Universität Tübingen
72076 Tübingen, Germany

G. Alsabeh, J. V. Milić
Laboratory of Photonics and Interfaces
Institute of Chemical Sciences and Engineering
École Polytechnique Fédérale de Lausanne
1015 Lausanne, Switzerland

D. Chernyshov
Swiss–Norwegian Beam Lines at the European Synchrotron Radiation Facility
European Synchrotron Radiation Facility (ESRF)
BP 220, 38000 Grenoble, France

A. Abate
Department of Novel Materials and Interfaces for Photovoltaic Solar Cells
Helmholtz-Zentrum Berlin für Materialien und Energie
Kekuléstraße 5, 12489 Berlin, Germany

A. Abate
Department of Chemistry
Bielefeld University
Universitätsstraße 25, 33615 Bielefeld, Germany

## 2. Results and Discussion

### 2.1. Material Design

Perfluoroarenes are expected to extrinsically stabilize perovskite materials with their enhanced hydrophobicity and provide an intrinsic stabilization of layered (2D) perovskite structure through π-based noncovalent interactions.[20,23] We apply perfluoroarenes to form 2D and treat 3D Sn perovskite phases, aiming to further improve the interface between the perovskite and selective charge transport layer in solar cells through increased hydrophobicity and passivating the interface defects.[20,24,25] Furthermore, perfluoroarene-based perovskites featured larger bandgaps compared with arene analogues,[20,24,25] potentially offering better energetic alignment. The perfluoroarenes were prepared by reducing tetrafluoroterephthalonitrile or pentafluorobenzonitrile precursors, followed by protonation of the resulting amines, as described in Experimental Section of the Supporting Information (Figure S1–S6, Supporting Information).

### 2.2. Perfluoroarene-Based 2D and Mixed-Dimensional Tin Perovskites

Perfluoroarene-based 2D Sn perovskites were prepared by solution processing via spin-coating and mechanosynthesis using ball-milling, as detailed in Experimental Section of the Supporting Information. For this purpose, we used stoichiometric quantities of $SnI_2$ and the corresponding spacer precursors, F-BNA and F-PDMA iodides, to form $n = 1$ nominal compositions of 2D perovskites. The RP phase, $(F\text{-}BNA)_2SnI_4$, was synthesized by reacting $SnI_2$ with (F-BNA)I in a molar ratio of 1:2, while the DJ phase $(F\text{-}PDMA)SnI_4$ was prepared using a 1:1 molar ratio of $SnI_2$ to $(F\text{-}PDMA)I_2$. For solution processing, we employed a solvent system composed of *N*,*N*-diethylformamide (DEF) and *N*,*N*′-dimethylpropyleneurea (DMPU) in a 1:6 volume ratio.[26,27] The $SnI_2$ and spacer precursors were dissolved in a dimethyl sulfoxide (DMSO)-free solvent mixture[26,27] and stirred for several hours to form a solution that was spin-coated on ITO substrate, followed by annealing at 100 °C to obtain 2D perovskite phases. In the case of mechanosynthesis of powders, $SnI_2$ and perfluoroarene spacer cation precursors were combined in stoichiometric amounts in a closed jar and ball-milled to form perovskite powders, which can be dissolved and processed to form the corresponding 2D perovskite films.[24,25,28–30]

The mechanosynthesis of the precursors resulted in homogeneous bright orange powders of $(F\text{-}BNA)_2SnI_4$ or $(F\text{-}PDMA)SnI_4$, and their solution processing led to the formation of the corresponding red films. The structural properties were investigated by XRD in the Bragg–Brentano configuration (**Figure 2**a–b). The XRD diffractograms of the $(F\text{-}BNA)_2SnI_4$ composition showed the presence of characteristic periodic patterns and low-angle reflections in the 2θ region below 10° that are associated with the basal (h00) planes of the 2D perovskites, demonstrating the efficacy of the F-BNA spacer to form well-defined layered perovskite structures (Figure 2a).[31] The 2D films also showed

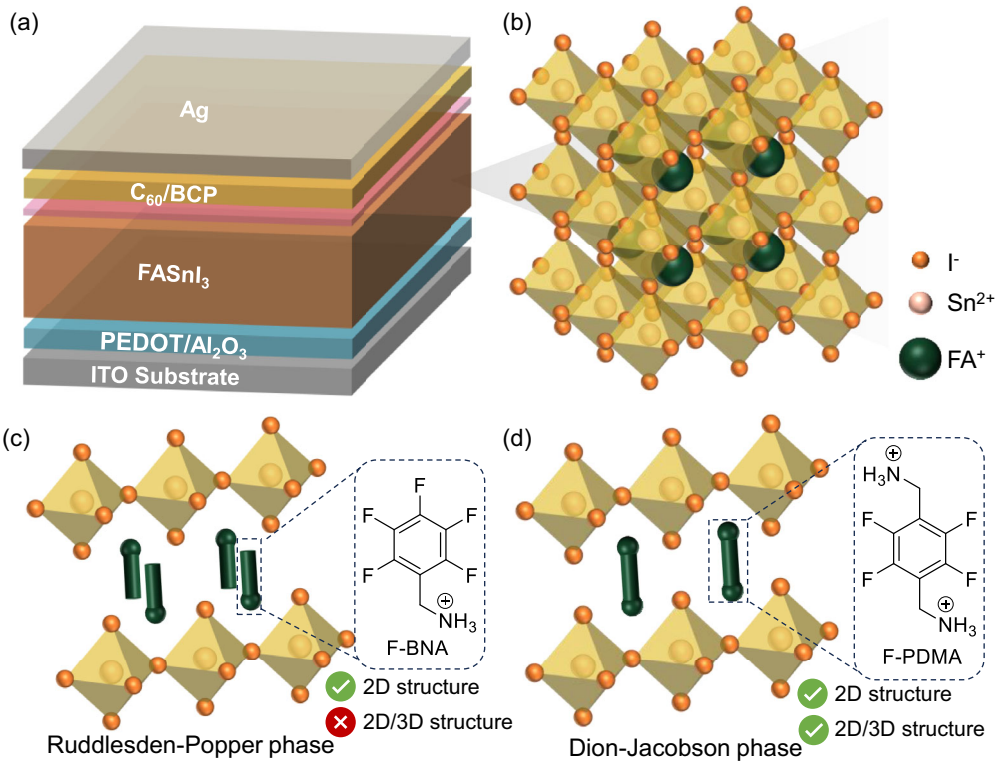


**Figure 1.** Schematic of the use of perfluoroarenes in tin perovskite photovoltaics. a) Structure of the p–i–n perovskite solar cell, where ITO is indium-doped tin oxide, PEDOT is poly(3,4-ethylenedioxythisphene), and BCP is bathocuproine. b) 3D $FASnI_3$ and c,d) 2D perovskite structures ($n = 1$ composition) of (c) RP and (d) DJ phases with the structural representation of organic cations as green rods, namely F-BNA and F-PDMA. While both spacers form 2D perovskite phases, only F-PDMA shows the formation of 2D/3D heterostructures.

small additional reflections (2θ at 6.6° and 7.1°) associated with oxidized Sn(II) species.[28] XRD patterns of (F-PDMA)$SnI_4$ revealed similar low-angle reflections and periodic patterns but with lower intensity compared to the RP phase (Figure 2b). In contrast, we obtained an increased crystallinity with mechanosynthetic powder used to prepare the DJ films (Figure 2b, insert). The DJ phase has a smaller lattice parameter associated with the spacer layer than the RP phase, per the expected characteristics (Figure 1c,d). To our knowledge, this was the first time to access a Sn-based DJ phase incorporating perfluoroarene cations. The structural properties were further analyzed by grazing incidence wide-angle X-ray scattering (GIWAXS) measurements of films (Figure S7, Supporting Information) to evidence the 2D structure. GIWAXS images indicated that $(F\text{-}BNA)_2SnI_4$ crystallized with a preferred orientation with the basal plane parallel to the substrate, whereas (F-PDMA)$SnI_4$ crystallized in with a random orientation. This can directly influence the optical properties and the potential for optoelectronic applications.[32]

The optical properties of the thin films were analyzed by UV–vis absorption and steady-state PL spectroscopy. The excitonic features in the absorption spectrum around 550 nm agree with the formation of 2D perovskite structures.[33] For $(F\text{-}BNA)_2SnI_4$ and (F-PDMA)$SnI_4$ thin films, the absorption peak was observed at 550 and 551 nm, respectively (Figure 2c,d). The PL spectra of $(F\text{-}BNA)_2SnI_4$ exhibited a minor Stokes shift of 20 nm, in accordance with the uniform perovskite film formation. In contrast, the Stokes shift of (F-PDMA)$SnI_4$ was higher (up to around 60 nm), likely associated with their lower crystallinity and the mixture of different orientations, as suggested by structural characteristics.

Having confirmed the 2D perovskite formation through optical and structural analysis, perfluoroarene spacers were applied to form mixed-dimensional perovskite heterostructures. Forming such heterostructures was found to be relevant for enhancing the stability and performance of perovskite-based devices.[34] The most common strategy to form a mixed-dimensional heterostructure is adding a low-dimensional overlayer by treating the 3D $FASnI_3$ perovskite surface with an organic spacer by solution processing. This allows the organic spacer to be incorporated into the 3D perovskite framework, forming a mixed-dimensional (e.g., 2D/3D) overlayer. Given the poor solubility of perfluoroarene spacers and the sensitive nature of Sn perovskites, we first investigated the solvent system most suitable for their processing (i.e., ethanol, isopropyl alcohol (IPA), 2-pentanol, diethyl ether, chlorobenzene, and toluene [Table S1, Supporting Information]). We further examined the effect of solvents that can dissolve perfluoroarene spacers through pure solvent surface treatment (Figure S8, Supporting Information). While ethanol treatment caused degradation of the perovskite layers—resulting in a complete failure of corresponding devices—IPA indicated a potential degradation of $FASnI_3$ layer. In contrast, 2-pentanol emerged as a more suitable solvent for surface treatment without any apparent degradation. Further analysis of solvent derivatives may enable optimizing the performance, which goes beyond the scope of this study. We have

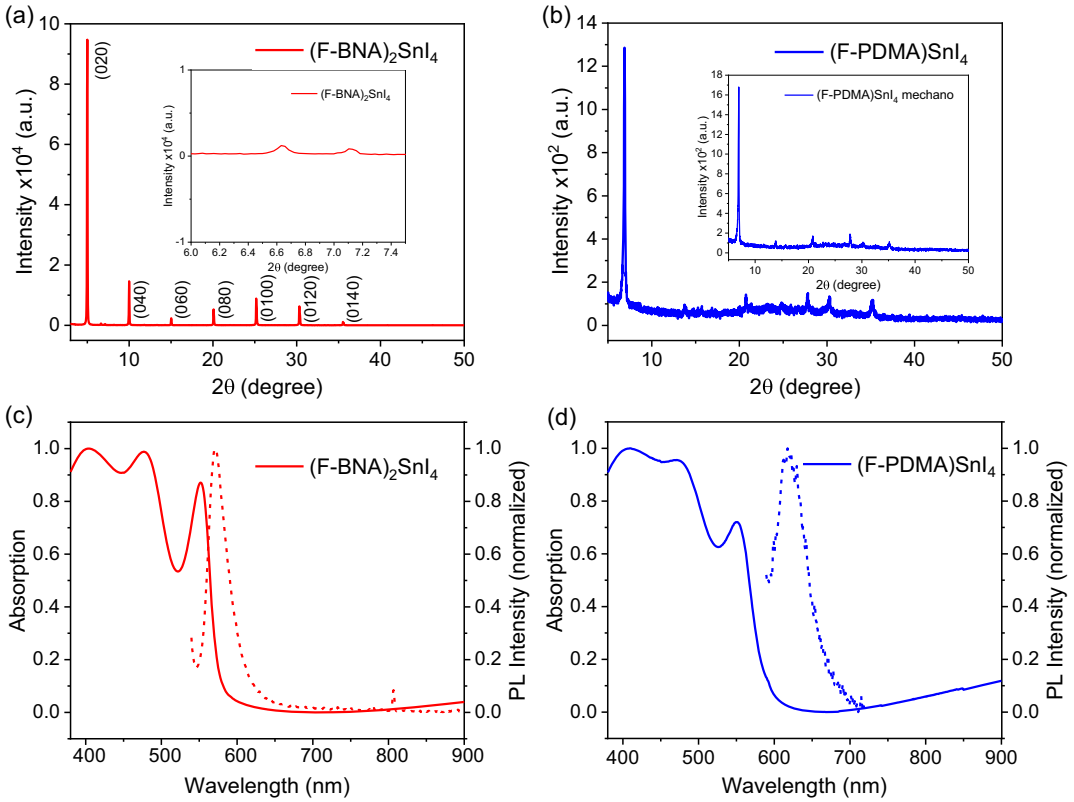


**Figure 2.** Structural and optical properties of perfluoroarene 2D tin perovskite films. a,b) XRD patterns and c,d) UV–vis absorption with PL spectra of (a,c) $(F\text{-}BNA)_2SnI_4$ and (b,d) $(F\text{-}PDMA)SnI_4$ thin films on microscope glass slides. Inset in (a) shows the magnified XRD pattern of 2θ between 6.0° and 7.5°. Inset in (b) shows an XRD pattern of $(F\text{-}PDMA)SnI_4$ thin films formed by using powders prepared mechanosynthetically.

studied both the untreated 3D perovskite films (referred to as *control*) and the 2-pentanol-treated ones (referred to as *pure*).

Scanning electron microscopy (SEM) images revealed that the control perovskite film, without surface treatment, exhibited apparent impurities on the surface. These impurities are likely to be associated with $SnI_2$ or $SnI_4$ as a result of using 10% stoichiometric excess of $SnI_2$ and the inevitable exposure to air before or during measurements, suggested by GIWAXS (Figure S11, Supporting Information). In contrast, 2-pentanol-treated perovskite films effectively removed impurities. XRD patterns (Figure S9, Supporting Information) also showed higher crystallinity of F-BNA-treated films. Furthermore, X-ray photoemission spectroscopy (XPS) measurements were carried out on the 3D and mixed-dimensional perovskite films (**Figure 3**e–g) to verify the existence of the perfluoroarene-based spacers on the 3D perovskites. The untreated (control) 3D perovskite films exhibited no detectable fluorine (F) signal, whereas a distinct F 1*s* core-level signal emerged at 687.9 eV for 2D/3D perovskite films (Figure 3e). Additionally, the nitrogen (N) 1*s* spectrum of the control 3D perovskite film featured characteristic C—N bonds (400.1 eV) associated with the FA cation (Figure 3f), whereas the F-PDMA-based films shifted the binding energies (by 0.1 eV), indicating interactions with spacers at the surface, similar to the C 1*s* XPS spectrum (Figure 3g). GIWAXS measurements confirmed 2D overlayer formation in F-PDMA-treated films in the resulting 2D/3D heterostructures, showing peaks at small q values of the same positions as in the 2D samples. In contrast, F-BNA-treated films did not show an apparent 2D signal (Figure S10, Supporting Information), suggesting that the organic spacer remained at the interface of treated perovskite films as a molecular interlayer. The resulting materials were thereafter applied to photovoltaic devices.

### 2.3. Application in Photovoltaics

The photovoltaic performance of tin hybrid perovskite with overlayers of perfluoroarene cations was investigated using devices with an architecture of ITO/PEDOT/$FASnI_3$/perfluoroarene/$C_{60}$/BCP/Ag (Figure 1a). In addition to treating the perovskite surface with (F-BNA)I and $(F\text{-}PDMA)I_2$, we also treated the surface with pure 2-pentanol, for comparison, to study the effects of solvent and perfluoroarene spacers, respectively. The devices treated with pure 2-pentanol (i.e., referred to as pure) exhibited higher short-circuit current densities ($J_{SC}$) and open-circuit voltage ($V_{OC}$) compared to untreated devices (referred to as control), although accompanied by a lower fill factor (FF). We attribute these performance changes to the surface-cleaning effect of 2-pentanol.[35,36] While solvent treatment can effectively remove impurities, it can also leave pinholes and vacancies on the surface, as apparent from the SEM images (Figure 3).[36] Notably, the pure devices demonstrated significantly improved photon-to-current efficiency (PCE) compared to the control devices, highlighting the role of 2-pentanol as an effective solvent for surface treatment (**Figure 4**). The champion pure device exhibited a

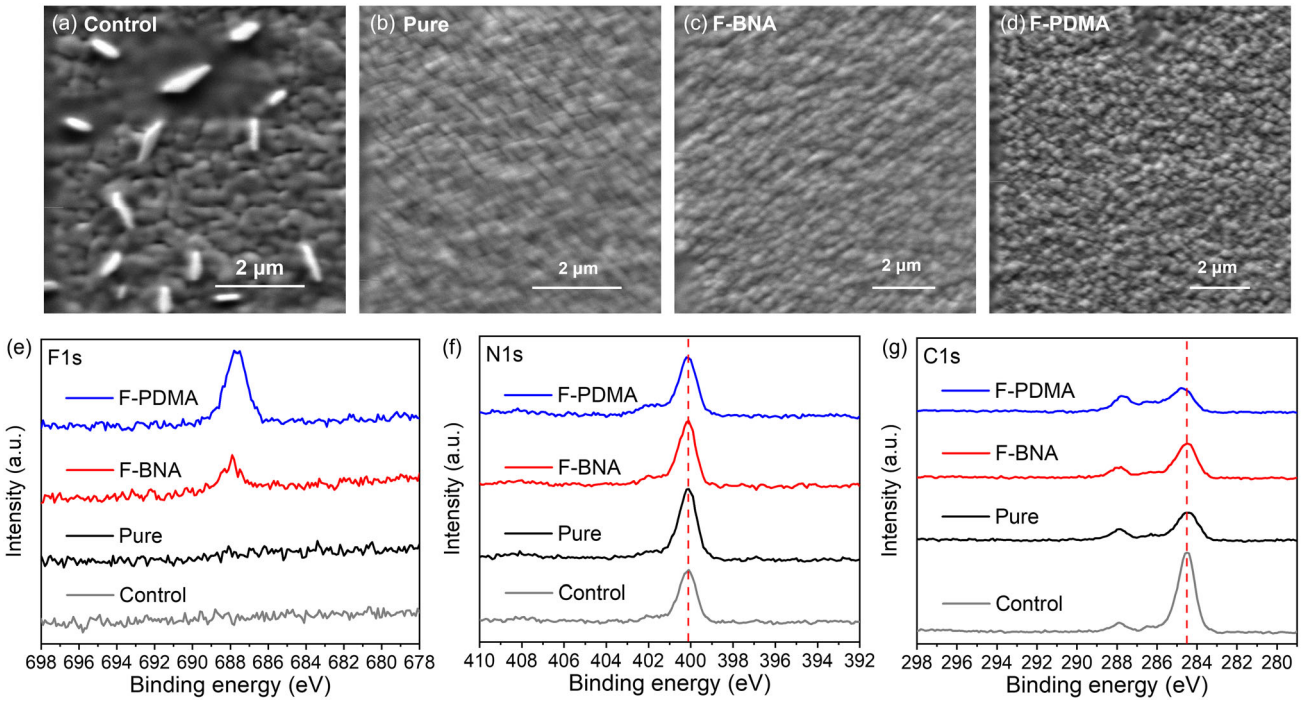


**Figure 3.** Morphology and interfacial properties of mixed-dimensional tin perovskite films. a–d) SEM images of the film surfaces based on (a) 3D films (Control), (b) 3D films treated with pure 2-pentanol (Pure), and (c,d) mixed-dimensional films treated with either (c) (F-BNA)I (labeled as F-BNA) and d) (F-PDMA)$I_2$ (labeled as F-PDMA). e–g) XPS F1s, N1s, and C1s core-level spectra of the 3D control (control, grey), 3D films treated with pure 2-pentanol (pure, black), and mixed-dimensional perovskite films with F-BNA (red) or F-PDMA (blue).

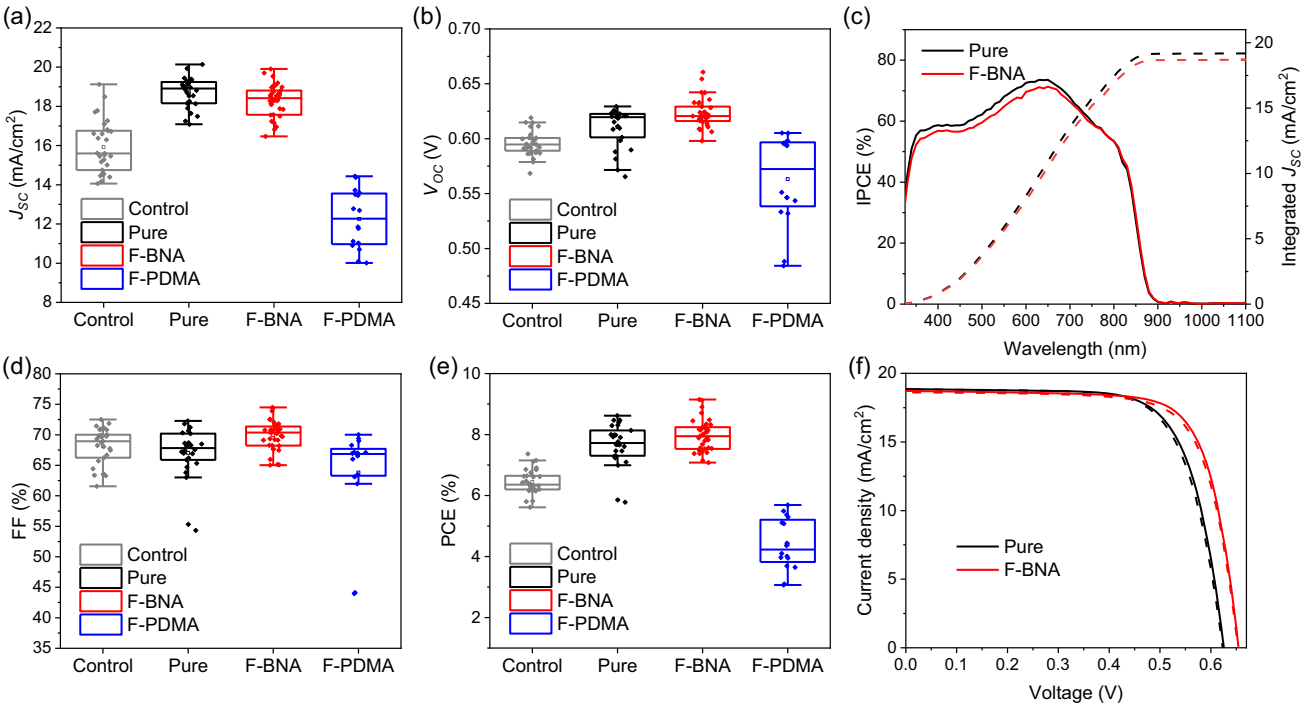


**Figure 4.** Photovoltaic performances in perfluoroarene-based tin perovskite solar cells. a,b and d,e) The statistical distribution of a) $J_{SC}$, b) $V_{OC}$, (d) FF, and IPCE for control (grey), pure (i.e., 2-pentanol-treated devices; black), F-BNA (red), and F-PDMA-treated devices (blue). c) IPCE spectrum of the champion control and F-BNA-treated devices with the projected photocurrent derived by integrating the IPCE over the spectral emission. f) *J–V* curves of the champion control and F-BNA-treated devices under the AM 1.5 G illumination.

**Table 1.** Photovoltaic performance of pure and F-BNA devices in forward and reverse scan direction.

| Device | | $V_{OC}$ [V] | $J_{SC}$ [mA cm$^{-2}$] | FF [%] | PCE [%] |
|---|---|---|---|---|---|
| Pure | Forward | 0.63 | 18.9 | 72 | 8.5 |
| | Reverse | 0.62 | 18.8 | 71 | 8.4 |
| F-BNAI | Forward | 0.65 | 18.7 | 75 | 9.1 |
| | Reverse | 0.65 | 18.6 | 74 | 9.0 |

higher $V_{OC}$ of 0.63 V, a higher $J_{SC}$ of 18.9 mA cm$^{-2}$, and a PCE of 8.5%, though a lower FF of 72% (**Table 1**). These enhancements showcase the effectiveness of 2-pentanol in optimizing performance. Furthermore, the effect of F-BNA and F-PDMA on the photovoltaic performance significantly differed. Specifically, while F-BNA treatment led to improved performance, F-PDMA treatment deteriorated power conversion efficiency. Moreover, F-BNA-treated devices exhibited improved $V_{OC}$ and FF, with only slightly reduced $J_{SC}$, which is likely due to surface passivation and better energetic alignment in agreement with previous reports on the role of fluorination.[24,37] Unlike pure treated systems, F-BNA was also found to improve the FF, indicating the relevance of molecular modulation compared to low-dimensional perovskite formation in photovoltaic performance. As a result, the average PCEs of control, pure, F-BNA, and F-PDMA 2D/3D perovskite devices were 6.4, 7.7, 7.9, and 4.2%, respectively. However, the champion F-BNA device reached a $V_{OC}$ of 0.65 V and a PCE of 9.1%, demonstrating the effectiveness in photovoltaics (Table 1). The current density obtained by integrating the incident photon-to-current efficiency (IPCE) as a function of wavelength for the champion device, 18.7 mA cm$^{-2}$, was in good agreement with the values from the current–voltage characteristics (18.7 mA cm$^{-2}$), excluding spectral mismatches.

We performed complementary optoelectronic characterization, including time-resolved PL and ultraviolet photoemission spectroscopy (UPS) to assess the photovoltaic performance improvement. Pure-treated films exhibited increased lifetimes compared to control 3D films (Figure S12, Supporting Information), consistent with the surface cleaning effect observed in SEM images, where impurities were effectively removed. F-PDMA-treated films displayed increased lifetimes compared with pure-treated films but featured lower $V_{OC}$, attributed to the lack of preferred orientation of the 2D/3D overlayer and dipole effects. This is likely related to the barrier from the distorted F-PDMA-based overlayer, including the insulating organic spacer barrier and potential barrier from disordered 2D DJ structures.[10] In contrast, F-BNA-treated films showed the highest $V_{OC}$, which was expected to exhibit extended carrier lifetimes due to surface passivating effects. However, they showed a decreased lifetime, likely due to the oxidation of $(F\text{-}BNA)_2SnI_4$ during the measurement. UPS analysis corroborates this behavior; while solvent treatments beneficially modified the work function and energy levels, enhancing charge extraction efficiency (**Figure 5**), the effect was not as apparent for the F-BNA-treated surfaces. In contrast, F-PDMA-based 2D/3D films exhibited undesired upward shift in the work function, suggesting the trend in the performance relates to changes in the interfacial energetics.

The effect of the perfluoroarene overlayer on the operational stability of unencapsulated devices was further analyzed by monitoring the shelf-life stability (Figure S13a, Supporting Information) and the evolution of their maximum power point (MPP) under continuous irradiation of 1 sun in a nitrogen atmosphere (Figure S13b, Supporting Information). The perfluoroarenes were expected to increase the hydrophobicity at the perovskite interface, as previously suggested,[20,24,25] which was thus not precisely evaluated in this case, such as by using contact angle measurements due to sensitivity in air. During the initial 200 h of storage, pure and F-BNA devices exhibited increased PCE, primarily as enhanced $J_{SC}$. The F-BNA device decreased to 87.5% of the initial efficiency after 50 days, yet the pure device retained 99% of the initial efficiency. This was corroborated by the MPP tracking measurements, revealing that pure devices exhibited higher stability than F-BNA-treated ones. After 1 h of operation, the F-BNA devices experienced a decline in performance to ≈81.5% of their initial value, while the pure

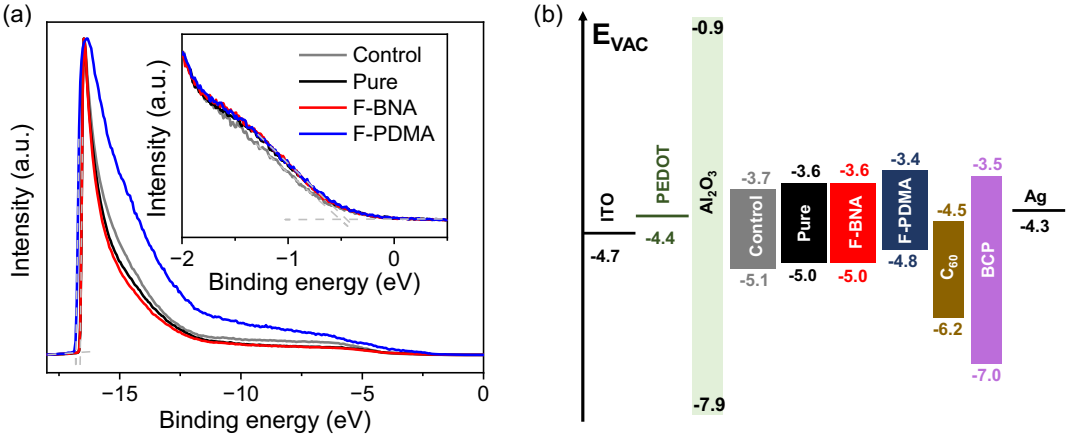


**Figure 5.** Energy band bending of mixed-dimensional perovskite films. a) UPS spectra of the 3D control (control, grey), 3D films treated with pure 2-pentanol (pure, black), and films with either F-BNA (red) or F-PDMA (blue) overlayers. b) Energy level diagram representation. Contact layer (electrode and charge-extraction layers) levels are based on ref. [22].

devices maintained around 90% of their initial performance. We attribute this to the effect of oxidation,[38] which was apparent by monitoring 2D $(F\text{-}BNA)_2SnI_4$ and 3D films by XRD (Figure S13c–d, Supporting Information), showcasing that $(F\text{-}BNA)_2SnI_4$ decomposed more rapidly after exposure to air for 15 min. A comparable characteristic is expected for the molecular overlayer. This challenges the conventional perspective of the role of molecular and mixed-dimensional overlayers in tin perovskite photovoltaics, which are commonly expected to increase the stability of solar cells, especially in 2D/3D perovskite compositions,[13–19] even in air.[39] In contrast, under the applied (DMSO-free) experimental conditions,[26,27] they were proven more effective in the overall photovoltaic performances yet compromising the resulting stability. This highlights the unique role of perfluoroarene moieties in low-dimensional tin perovskites and the more significant importance of solvent-mediated surface treatments in tin perovskite photovoltaics, such as through catalytic effect in forming mixed-dimensional heterostructures or other,[40] which stimulates further investigations to unravel the underlying design principles in the future.

## 3. Conclusion

We applied perfluoroarene cations, specifically F-BNA and F-PDMA, to form RP and, for the first time, DJ 2D hybrid perovskites, respectively. Structural and optoelectronic characterizations confirmed the formation of 2D tin perovskite phases. These perfluoroarene moieties were then applied to create mixed-dimensional perovskite overlayers using 2-pentanol via surface treatment of 3D $FASnI_3$ perovskite materials. While F-PDMA-based overlayers formed 2D/3D perovskite heterostructures, F-BNA treatment resulted in interfacial molecular modulation, which is possibly due to different steric hindrance and functionality that is more likely to form 2D overlayers for bifunctional F-PDMA spacer cations.[41] The resulting materials were incorporated into p–i–n perovskite solar cells, demonstrating improved photovoltaic performance with a champion PCE of up to 9.1% for F-BNA-treated devices. Notably, the champion devices achieved a $V_{OC}$ of 0.654 V, representing a 10% increase compared to control devices, attributed to solvent surface cleaning and F-BNA passivating effects. In contrast, F-PDMA-based 2D/3D perovskite heterostructures exhibited reduced photovoltaic performance, which is likely due to their unfavorable surface energetics.[17] This study challenges the conventional role of mixed-dimensional perovskite overlayers in tin perovskite photovoltaics, increasing performances for molecular overlayers compared to mixed-dimensional perovskite heterostructures, yet at the expense of operational stabilities. Moreover, it showcases the unique role of perfluoroarene cations and the importance of solvent treatments. This sets the basis for future research toward optimizing crystallization and device engineering to enhance performance and stability, paving the way for more effective tin perovskite photovoltaics.

## Supporting Information

Supporting Information is available from the Wiley Online Library or from the author.

## Acknowledgements

M.Z. and J.V.M. are grateful to the Chinese Scholarship Council (CSC) for financial support (grant no. 202306380063) and Adolphe Merkle Institute at the University of Fribourg for supporting this research. J.V.M. appreciates the support of the Swiss National Science Foundation PRIMA project no. 193174. The authors acknowledge the European Synchrotron Radiation Facility (ESRF) for providing synchrotron radiation facilities under proposal number MA-6012. We also acknowledge funding from the BMBF (ERUM-Pro) project 05K19VTA. S. S. and Y. V. also acknowledge HORIZON-MSCA-2021-PF-01-01 no. 101066273 from the European Commission for funding this project. Y.V. thanks the Leibniz Programme for Women Professors for funding (SUPERSOL, P144/2022). J-Y.S. is supported by Basic Science Research Program through the National Research Foundation of Korea (NRF) funded by the Ministry of Education RS-2022-NR073004. We are grateful to Prof. Ullrich Steiner (Adolphe Merkle Institute) for his support throughout the project.

## Conflict of Interest

The authors declare no conflict of interest.

## Author Contributions

**Mengqiong Zhu**: data curation (lead); funding acquisition (supporting); investigation (lead); methodology (equal); writing—original draft (lead); and writing—review and editing (lead). **Shivam Singh**: investigation (supporting); methodology (supporting); and writing—review and editing (supporting). **Alejandra Maria Castro Chong**: investigation (equal); methodology (supporting); and writing—review and editing (supporting). **Jong-Min Kim**: investigation (supporting) and writing—review and editing (supporting). **Fulya Koc**: investigation (supporting); methodology (supporting); and writing—review and editing (supporting). **Debendra Prasad Panda**: investigation (supporting); methodology (supporting); and writing—review and editing (supporting). **Paul Zimmermann**: data curation (supporting); investigation (supporting); methodology (supporting); and writing—review and editing (supporting). **Alexander Hinderhofer**: funding acquisition (supporting); investigation (supporting); methodology (supporting); supervision (supporting); and writing—review and editing (supporting). **Weifan Luo**: investigation (supporting); methodology (supporting); and writing—review and editing (supporting). **Ghewa Alsabeh**: investigation (supporting); methodology (supporting); and writing—review and editing (supporting). **Muhammad Okash Ur Rehman**: investigation (supporting); methodology (supporting); and writing—review and editing (supporting). **Gyeongcheon Choi**: investigation (supporting); methodology (supporting); and writing—review and editing (supporting). **Dmitry Chernyshov**: methodology (supporting); supervision (supporting); and writing—review and editing (supporting). **Frank Schreiber**: funding acquisition (supporting); methodology (supporting); supervision (supporting); and writing—review and editing (supporting). **Ji-Youn Seo**: methodology (supporting); supervision (supporting); and writing—review and editing (supporting). **Yana Vaynzof**: methodology (supporting); supervision (supporting); and writing—review and editing (supporting). **Antonio Abate**: funding acquisition (supporting); investigation (supporting); project administration (supporting); supervision (equal); and writing—review and editing (supporting). **Jovana V. Milić**: conceptualization (lead); funding acquisition (supporting); supervision (lead); writing—original draft (supporting); and writing—review and editing (lead).

## Data Availability Statement

Data presented here can be accessed at the following DOI:10.5281/zenodo.15110945, and it is available under the license CC-BY-4.0 (Creative Commons Attribution-ShareAlike 4.0 International).

## Keywords

perfluoroarenes, perovskite solar cells, solvent engineering, tin halide perovskites

Received: February 25, 2025
Revised: March 18, 2025
Published online: April 30, 2025

[1] J. Li, H.-L. Cao, W.-B. Jiao, Q. Wang, M. Wei, I. Cantone, J. Lü, A. Abate, *Nat. Commun.* **2020**, *11*, 310.
[2] K. P. Goetz, A. D. Taylor, Y. J. Hofstetter, Y. Vaynzof, *ACS Appl. Mater. Interfaces* **2021**, *13*, 1.
[3] A. Abate, *ACS Energy Lett.* **2023**, *8*, 1896.
[4] P. V. Kamat, J. Bisquert, J. Buriak, *ACS Energy Lett.* **2017**, *2*, 904.
[5] J. Zhao, Z. Zhang, G. Li, M. H. Aldamasy, M. Li, A. Abate, *Adv. Energy Mater.* **2023**, *13*, 2204233.
[6] G. Nasti, M. H. Aldamasy, M. A. Flatken, P. Musto, P. Matczak, A. Dallmann, A. Hoell, A. Musiienko, H. Hempel, E. Aktas, D. Di Girolamo, J. Pascual, G. Li, M. Li, L. V. Mercaldo, P. D. Veneri, A. Abate, *ACS Energy Lett.* **2022**, *7*, 3197.
[7] F. Yang, R. Zhu, Z. Zhang, Z. Su, W. Zuo, B. He, M. H. Aldamasy, Y. Jia, G. Li, X. Gao, Z. Li, M. Saliba, A. Abate, M. Li, *Adv. Mater.* **2024**, *36*, 2308655.
[8] Y. Shi, Z. Zhu, D. Miao, Y. Ding, Q. Mi, *ACS Energy Lett.* **2024**, *9*, 1895.
[9] M. Aldamasy, Z. Iqbal, G. Li, J. Pascual, F. Alharthi, A. Abate, M. Li, *Phys. Chem. Chem. Phys.* **2021**, *23*, 23413.
[10] G. Grancini, M. K. Nazeeruddin, *Nat. Rev. Mater.* **2019**, *4*, 4.
[11] N. Mercier, *Angew. Chem. Int. Ed.* **2019**, *58*, 17912.
[12] F. Wang, X. Jiang, H. Chen, Y. Shang, H. Liu, J. Wei, W. Zhou, H. He, W. Liu, Z. Ning, *Joule* **2018**, *2*, 2732.
[13] K. Chen, P. Wu, W. Yang, R. Su, D. Luo, X. Yang, Y. Tu, R. Zhu, Q. Gong, *Nano Energy* **2018**, *49*, 411.
[14] L. Wang, H. Bi, J. Liu, Y. Wei, Z. Zhang, M. Chen, A. K. Baranwal, G. Kapil, T. Kitamura, S. Yang, Q. Miao, Q. Shen, T. Ma, S. Hayase, *ACS Energy Lett.* **2024**, *9*, 6238.
[15] Z. Zhu, X. Jiang, D. Yu, N. Yu, Z. Ning, Q. Mi, *ACS Energy Lett.* **2022**, *7*, 2079.
[16] S. Shao, M. Nijenhuis, J. Dong, S. Kahmann, G. H. Ten Brink, G. Portale, M. A. Loi, *J. Mater. Chem. A* **2021**, *9*, 10095.
[17] E. Jokar, P.-Y. Cheng, C.-Y. Lin, S. Narra, S. Shahbazi, E. Wei-Guang Diau, *ACS Energy Lett.* **2021**, *6*, 485.
[18] J. Dong, S. Shao, S. Kahmann, A. J. Rommens, D. Hermida-Merino, G. H. ten Brink, M. A. Loi, G. Portale, *Adv. Funct. Mater.* **2020**, *30*, 2001294.
[19] S. Shao, J. Liu, G. Portale, H.-H. Fang, G. R. Blake, G. H. ten Brink, L. J. A. Koster, M. A. Loi, *Adv. Energy Mater.* **2018**, *8*, 1702019.
[20] J. V. Milić, *J. Phys. Chem. Lett.* **2022**, *13*, 9869.
[21] B.-B. Yu, Z. Chen, Y. Zhu, Y. Wang, B. Han, G. Chen, X. Zhang, Z. Du, Z. He, *Adv. Mater.* **2021**, *33*, 2102055.
[22] D. Di Girolamo, E. Aktas, C. Ponti, J. Pascual, G. Li, M. Li, G. Nasti, F. Alharthi, F. Mura, A. Abate, *Mater. Adv.* **2022**, *3*, 9083.
[23] W. Luo, G. AlSabeh, J. V. Milic, *Photochemistry* (Eds: S. Crespi, S. Protti), Royal Society Of Chemistry, Cambridge **2022**, pp. 346–370.
[24] M. A. Hope, T. Nakamura, P. Ahlawat, A. Mishra, M. Cordova, F. Jahanbakhshi, M. Mladenović, R. Runjhun, L. Merten, A. Hinderhofer, B. I. Carlsen, D. J. Kubicki, R. Gershoni-Poranne, T. Schneeberger, L. C. Carbone, Y. Liu, S. M. Zakeeruddin, J. Lewinski, A. Hagfeldt, F. Schreiber, U. Rothlisberger, M. Grätzel, J. V. Milić, L. Emsley, *J. Am. Chem. Soc.* **2021**, *143*, 1529.
[25] M. Almalki, A. Dučinskas, L. C. Carbone, L. Pfeifer, L. Piveteau, W. Luo, E. Lim, P. A. Gaina, P. A. Schouwink, S. M. Zakeeruddin, J. V. Milić, M. Grätzel, *Nanoscale* **2022**, *14*, 6771.
[26] D. Di Girolamo, J. Pascual, M. H. Aldamasy, Z. Iqbal, G. Li, E. Radicchi, M. Li, S.-H. Turren-Cruz, G. Nasti, A. Dallmann, F. De Angelis, A. Abate, *ACS Energy Lett.* **2021**, *6*, 959.
[27] E. Aktas, I. Poli, C. Ponti, G. Li, A. Olivati, D. Di Girolamo, F. A. Alharthi, M. Li, E. Palomares, A. Petrozza, A. Abate, *ACS Energy Lett.* **2023**, *8*, 5170.
[28] J. V. Milić, J. Im, D. J. Kubicki, A. Ummadisingu, J. Seo, Y. Li, M. A. Ruiz-Preciado, M. I. Dar, S. M. Zakeeruddin, L. Emsley, M. Grätzel, *Adv. Energy Mater.* **2019**, *9*, 1900284.
[29] A. Ummadisingu, A. Mishra, D. J. Kubicki, T. LaGrange, A. Dučinskas, M. Siczek, W. Bury, J. V. Milić, M. Grätzel, L. Emsley, *Small* **2022**, *18*, 2104287.
[30] J. V. Milić, S. M. Zakeeruddin, M. Grätzel, *Acc. Chem. Res.* **2021**, *54*, 2729.
[31] L. Mao, C. C. Stoumpos, M. G. Kanatzidis, *J. Am. Chem. Soc.* **2019**, *141*, 1171.
[32] S.-J. Kim, R. Kumar Chitumalla, J.-M. Kim, J. Jang, J.-W. Oh, J. V. Milić, J.-Y. Seo, *Helv. Chim. Acta* **2023**, *106*, e202200193.
[33] J.-C. Blancon, J. Even, C. C. Stoumpos, M. G. Kanatzidis, A. D. Mohite, *Nat. Nanotechnol.* **2020**, *15*, 969.
[34] H. Zhu, J. Ma, P. Li, S. Zang, Y. Zhang, Y. Song, *Chem* **2022**, *8*, 2939.
[35] J. Wang, K. Wang, C. Zhang, S. Liu, X. Guan, C. Liang, C.-C. Chen, F. Xie, *Adv. Energy Mater.* **2023**, *13*, 2302169.
[36] W. Cai, Y. Wang, W. Li, Y. Yin, J. Liu, W. Cai, S. Wang, J. Guo, S. Chang, S. Li, X. Wang, Y. Shi, *Adv. Energy Mater.* **2024**, *14*, 2304521.
[37] S.-H. Turren-Cruz, J. Pascual, S. Hu, J. Sanchez-Diaz, S. Galve-Lahoz, W. Liu, W. Hempel, V. S. Chirvony, J. P. Martinez-Pastor, P. P. Boix, A. Wakamiya, I. Mora-Seró, *ACS Energy Lett.* **2024**, *9*, 432.
[38] D. Yu, M. Pan, G. Liu, X. Jiang, X. Wen, W. Li, S. Chen, W. Zhou, H. Wang, Y. Lu, M. Ma, Z. Zang, P. Cheng, Q. Ji, F. Zheng, Z. Ning, *Nat. Energy* **2024**, *9*, 298.
[39] M. Sun, M. Ma, Y. Guo, S. Yuan, H. Xiong, Z. Tan, W. Li, J. Fan, Z. Ning, *Sol. RRL* **2022**, *6*, 2200672.
[40] J. Xi, J. Jiang, H. Duim, L. Chen, J. You, G. Portale, S. Liu, S. Tao, M. A. Loi, *Adv. Mater.* **2023**, *35*, 2302896.
[41] S. Teale, M. Degani, B. Chen, E. H. Sargent, G. Grancini, *Nat. Energy* **2024**, *9*, 779.